SOUTHWEST RESEARCH INSTITUTE®

6220 CULEBRA RD. 78238-5166 • P.O. DRAWER 28510 78228-0510 • SAN ANTONIO, TEXAS, USA • (210) 684-5111 • WWW.SWRI.ORG

Applied Physics Division
30 January 2007

Ms. Emily Richardson
South Florida Water Management District
SFWMD: Headquarters B-2 Building
3301 Gun Club Road
West Palm Beach, FL 33406

Re: Final Report, SwRI Project No. 14-12583
"Analysis and Interpretation of Crosswell Seismic and Well Logs for Estimating Lateral Porosity and Permeability Variations in the Interwell Region Between Wells MF-37 and EXPM-1 at the Port Mayaca Site, South Florida,"

Dear Ms. Richardson:

Please find enclosed one spiral-bound copy and one CD, both containing the above referenced final report. Also enclosed, in a separate package, is one spiral-bound copy of the report for Mr. Ryan Patrick. Would you please forward this package on to him.

It has been a pleasure to work on this project. If you have any questions about the report, please do not hesitate to call me at (210) 522-3284.

Sincerely,

Jorge Parra, Ph.D., Institute Scientist

APPROVED BY:

Ed Moore, Vice President
Applied Physics Division

HOUSTON, TEXAS (713) 977-1377 • WASHINGTON, DC (301) 881-0226

ANALYSES AND INTERPRETATION OF CROSSWELL SEISMIC AND WELL LOGS FOR ESTIMATING LATERAL POROSITY AND PERMEABILITY VARIATIONS IN THE INTERWELL REGION BETWEEN WELLS MF-37 AND EXPM-1 AT THE PORT MAYACA SITE, SOUTH FLORIDA

Final Report

SwRI Project 14-12583
Purchase Order ID 4500000586

Prepared for:

South Florida Water Management District
SFWMD: Headquarters B-2 Building
3301 Gun Club Road
West Palm Beach, Florida 33406

JANUARY 2007

ANALYSES AND INTERPRETATION OF CROSSWELL SEISMIC AND WELL LOGS FOR ESTIMATING LATERAL POROSITY AND PERMEABILITY VARIATIONS IN THE INTERWELL REGION BETWEEN WELLS MF-37 AND EXPM-1 AT THE PORT MAYACA SITE, SOUTH FLORIDA

Final Report

SwRI Project 14-12583
Purchase Order ID 4500000586

Prepared for:

South Florida Water Management District
SFWMD: Headquarters B-2 Building
3301 Gun Club Road
West Palm Beach, Florida 33406

Prepared by:

Jorge Parra, Ph.D.
Institute Scientist

JANUARY 2007

APPROVED:

Ed Moore, Vice President
Applied Physics Division

TABLE OF CONTENTS

LIST OF FIGURES

ANALYSES AND INTERPRETATION OF CROSSWELL SEISMIC AND WELL LOGS FOR ESTIMATING LATERAL POROSITY AND PERMEABILITY VARIATIONS IN THE INTERWELL REGION BETWEEN WELLS MF-37 AND EXPM-1 AT THE PORT MAYACA SITE, SOUTH FLORIDA

ABSTRACT

High-resolution seismic reflection between wells provides images of the subsurface about one order of magnitude greater than surface seismic reflection. The cross-well seismic images have outlined the zones of high matrix porosity and permeability that are associated with high water production at the Port Mayaca test site. The top of the Floridan Aquifer System and the lower boundary of the intermediate confining unit (the basal Hawthorn) are delineated with the impedance image. The spectral waveform analyses have identified one heterogeneous zone at the interval from 900 to 950 ft. In this interval, the relationship between well logs and the zero vertical offset waveforms suggests that the wave attenuation is due to scattering associated with the vertical variability of the secondary and primary porosity sequence. The impedance, porosity and permeability images captured the variation of the aquifer matrix in the interwell region. In particular, the impedance image provides the stiff and soft zones of the aquifer. The stiff zones contain conduits that may not be connected, which are associated with secondary porosity features such as pore/vugs/fractures near the wells. The soft zones of low impedance are associated with high water production. Furthermore, the impedance and porosity images, combined with the Formation Micro Scanner Image (FMI) image logs, have provided information that can explain the development of conduits in the stiff intervals. The permeability image gives a good visualization of low and high matrix permeability distribution intervals. The FMI image data provides information on the secondary porosity distribution at the borehole scale that cannot be detected with any other log. In particular, the FMI image logs have showed a sequence of dark (conductive) and white (resistive) bands. This suggests that the conductive bands are porous and saturated with salt water (high permeability spikes). Some of the resistive bands may be connected between wells, but the dark zones embedded in the white bands are not. Zones characterized by these sequences are intervals with low water production.

I. INTRODUCTION

A. Background

A crosswell survey was conducted at the Port Mayaca test site, which is about 30 miles west of the Atlantic Ocean and approximately one mile east of the eastern boundary of Lake Okeechobee in Martin County, Florida. The measurements were taken between monitoring wells MF-37 and EXPM-1, at an interwell separation of 1300 ft., using a Z-Seis piezoceramic X series source and a 10-level hydrophone system (Parra et al., 2003). Multiple source and detector measurements were taken in the interval from 400 to 1700 ft. Figure 1 shows the velocity tomography image, and Figure 2 shows the crosswell reflection data. The objectives of the survey were to map the flow units' variability in the region between the two wells, to assess whether the high-resolution seismic survey could resolve and detect zones of high water production, and to map the matrix porosity/permeability. To reach these objectives, we integrated well log data to generate impedance, permeability, and porosity images of the interwell region as well as to provide an interpretation with Formation Micro Scanner Image (FMI) images and petrophysics.

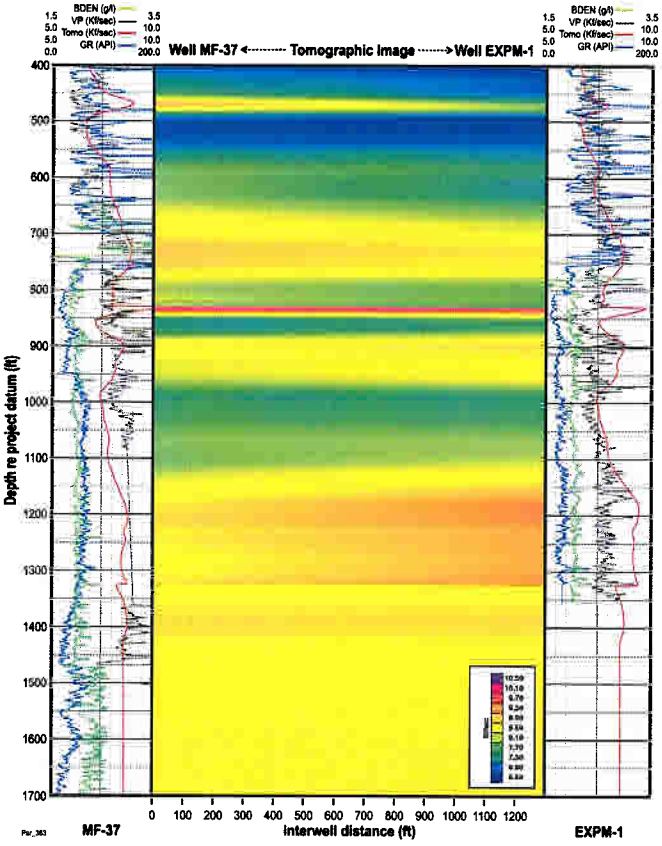

FIGURE 1. Velocity tomography image correlated with well logs from MF-37 and EXPM-1 wells.

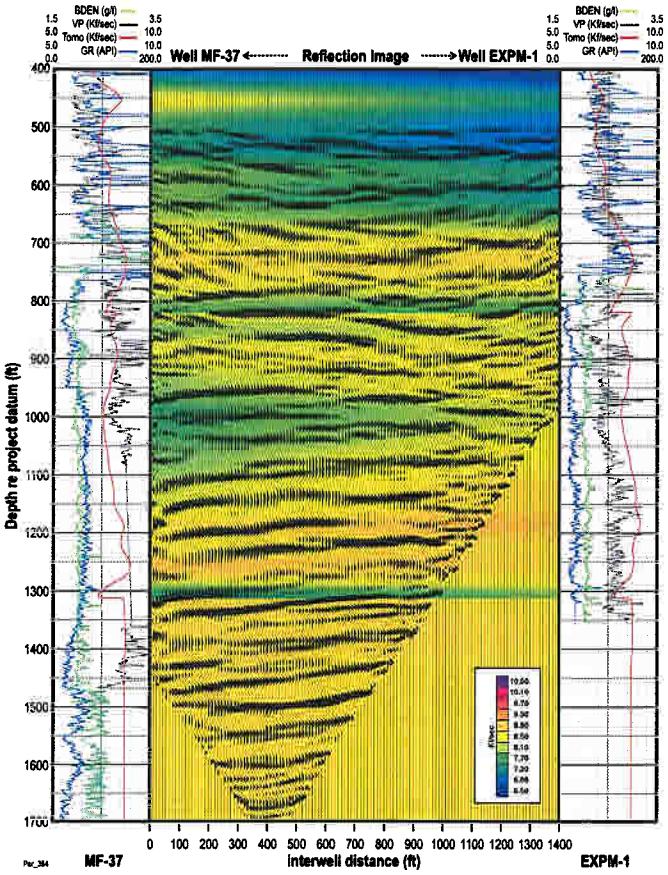

FIGURE 2. Crosswell reflection seismic data correlated with well logs from MF-37 and EXPM-1 wells.

Important information relevant to the analysis was obtained from the report by Bennett and Rectenwald (2002). In this report, the top of the Florida Aquifer System (FAS) is identified at a depth of 755 ft. The lithologic and geophysical logs and packer test results from well MF-37 indicate moderate production capacity of the upper Floridan aquifer from 755 to 1300 ft. The aquifer's intermediate confining unit (extends from 146 -755 ft.) is formed by clay, silt and mudstone, and the aquifer system is formed by: (a) wackestone and packstone in the interval from 750 to 1050 ft., and (b) wackestone and mudstone below 1050 ft.

The confining unit exhibits a change in lithology from a clay-silt unit to a predominantly porous, moderately indurate carbonate unit below 430 ft. This zone is identified as the Arcadia Formation and it contains intervals of significant phosphate sand/silt content with thin, intermittent, moderately indurated limestone units identified by positive spikes in the resistivity and sonic logs. Later in this report, we will address the presence of these features in more detail. The top of the basal Hawthorn unit, which marks the lower boundary of the Arcadia Formation, was identified at 715 ft. in well MF-37 and at 725 ft. in well EXPM-1. This boundary was identified using the impedance image based on the crosswell data. The Hawthorn unit consists of yellowish-gray packstone with significant carbonate mud content from 725 to 755 ft., which limits this interval's vertical and horizontal permeability. The low-permeability intervals below

the Hawthorn unit (in the lower boundary of the Arcadia Formation) were delineated by the crosswell image data as well.

The top of the FAS is part of the Arcadia Formation in the region of 755 to 790 ft. The FAS consists of moderately indurated packstone and grainstone units containing shell fragments and phosphate sands and silts. The dual induction, sonic, and caliper logs indicated a competent low porosity unit at 755-790 ft., where the resistivity increased from 12 to 40 Ohm-m.

A sharp formation contact between the Arcadia Formation and the Suwannee Limestone at 790 ft. was identified by a change in lithology from dark gray to yellowish-gray packstone. This discontinuity was associated with a decrease in formation resistivity and sonic velocity.

The fluid-type logs indicated good water production from flow zones in the intervals from 800 to 900 ft. and from 925 to 1030 ft. Below 1030 ft., the productive capacity is limited, suggesting lower permeability, semi-confining units near the base of the storage horizon.

B. Project Summary

We reviewed the crosswell seismic data and well logs from wells EXPM-1 and MF-37. Selected P-wave velocity and density logs were used to produce impedance images, and the band-limited inversion algorithm was applied to produce impedance (Parra et al, 2003). The algorithm allows constraint of the impedance inversion to match the well log impedance in the vicinity of both wells. Away from the wells, impedance was constrained by lateral continuity. To relate the impedance changes to the hydrological characteristics of the aquifer, we constructed cross plots of impedance at the borehole locations versus the porosity and permeability well logs. These plots were selected on the basis of the lithological information. We produced regression equations relating impedance to flow properties at the boreholes, and we used the resulting relationships to produce permeability and porosity images at the crosswell seismic scale. In addition, we performed a spectral analysis of the zero vertical offset crosswell data to identify high attenuation zones that may be related to permeable zones. Finally, we conducted an interpretation by integrating well logs with porosity and permeability images.

II. METHODOLOGY AND WELL LOG RESULTS

A. Review of Well Logs

Our main goal was to use the Stoneley wave permeability to generate cross plots and eventually to produce permeability images. Because the borehole conditions were poor due to the presence of large washouts, the Stoneley wave permeability was not reliable enough to be used in an analysis. Schlumberger tried to consolidate the Stoneley wave permeability into one robust estimate by using energy or semblance computation modes, transmitter versus receiver modes, etc. These methods did not work, so Schlumberger estimated permeability in different ways. One approach was based on the ELAN integrated log analysis, which optimizes mineral-pore volume using a mineral and a porosity equation. A second approach was application of the Timur-Coates equation, which uses secondary porosity (vug or fracture) estimated from the FMI resistivity image as the free water part of the equation, and matrix porosity from the FMI analysis as the bound water part of the equation. This means of estimating permeability assumes that the delineated secondary porosity is the main mechanism for permeability and the matrix porosity is well-connected. This assumption made sense for the FAS, in particular, where the narrow conduits are located, and the permeability logs were obtained from EXPM-1 and MF-37 FMI data. We decided to use the ELAN integrated log analysis to produce the crosswell images, and the Timur-Coates equation for correlation between well logs, as well as the final interpretation with the images.

The best estimate of total porosity was from the ELAN integrated log analyses (Ned Clayton, personal communication). However, two neutron porosities were derived in slightly different ways. These were NPOR, which is a resolution "enhanced" neutron porosity, and HNPO, which has the highest vertical resolution. Density porosity is another measurement of porosity, but it requires an assumption of matrix density. Very high resolution outputs from FMI resistivity analysis provided the secondary, matrix and total porosity logs. We used FMI ELAN to generate the porosity image from crosswell data.

B. Well Log Analyses

To generate porosity and permeability images, one must understand how to relate high-resolution log information to field-scale reflection seismic data. In fact, the vertical resolution of the crosswell reflection seismic is about 3 ft., and that of the sonic log is about 1 ft. To evaluate whether the crosswell reflection seismic data is detecting the pore structure in the interwell region, we need to estimate the relationship between the petrophysics and the well logs. Since the FMI images capture the limestone rock structure at the borehole scale, we considered these well log images as representing rock formation characteristics. Figure 3 shows a comparison of porosity and permeability logs with the FMI image of well EXMP-1. The logs on the left are the FMI secondary porosity (green), the FMI total porosity (red), and the ELAN porosity (solid). On the right are the FMI permeability log (orange) and the intrinsic permeability log (blue). In the middle is the FMI image log. The ELAN porosity logs have similar resolutions to the sonic logs, and they capture the matrix or primary porosity of the formation. The FMI image shows horizontal high resistive streaks, or a sharp decrease in conductivity. These tight limestones are

observed clearly in several places, at 1000, 930, 910, 860, and 830 ft.; these features correlate with the ELAN porosity. In addition, in the region between 900 and 950 ft., we observed several much thinner horizontal streaks that were not resolved by the ELAN porosity log, and nor could they be resolved by sonic logs.

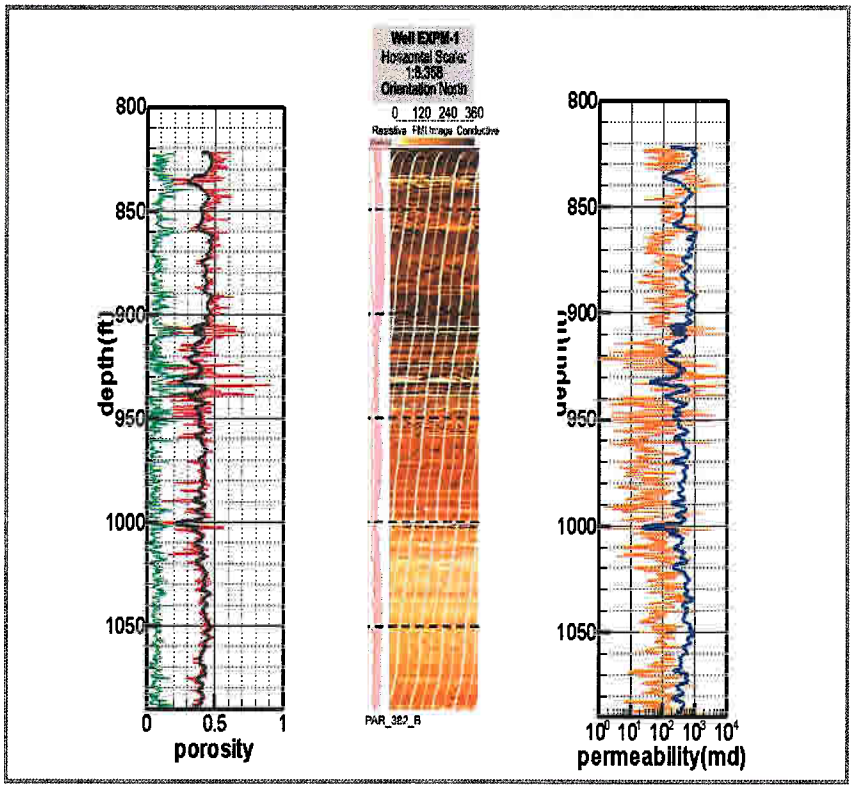

FIGURE 3. Comparison between the FMI image log and the porosity and permeability well logs of well EXPM-1. The porosity logs illustrate the effects of secondary porosity on matrix and total porosity. The dark log is the ELAN porosity. The last track shows the intrinsic permeability (blue) and KTIM permeability logs.

These thin streaks lowered ELAN porosity in the interval from 900 to 950 ft. However, between these resistive streaks there are thin, conductive limestone zones that are associated with higher resolution porosity corresponding to secondary porosity. In fact, the porosity spikes above the ELAN porosity are secondary porosity values, which may be due to fractures and/or interconnected vuggy porosity, and they correlate with high conductivity features in the FMI image.

The horizontal streaks correspond to low permeability markers, especially those that can be resolved with sonic logs and ELAN porosity logs. If we assume that the ELAN intrinsic permeability measures the matrix permeability, any permeability log that has permeability values greater than the intrinsic permeability may be associated with fluid flow in the conduits of the aquifer. This is clearly observed at 840 ft., near 910 ft., from 920 to 950 ft., and a little bit at 990 ft.

A similar interpretation can be done for well MF-37 in Figure 4. This FMI image log is, in general, less conductive than the FMI image of well EXPM-1, but this part of the formation has more secondary porosity than that intercepted by well EXPM-1. Consequently, the permeability associated with the secondary porosity is greater than the matrix permeability in this well, while the permeability and porosity of the matrix is consistent in both wells.

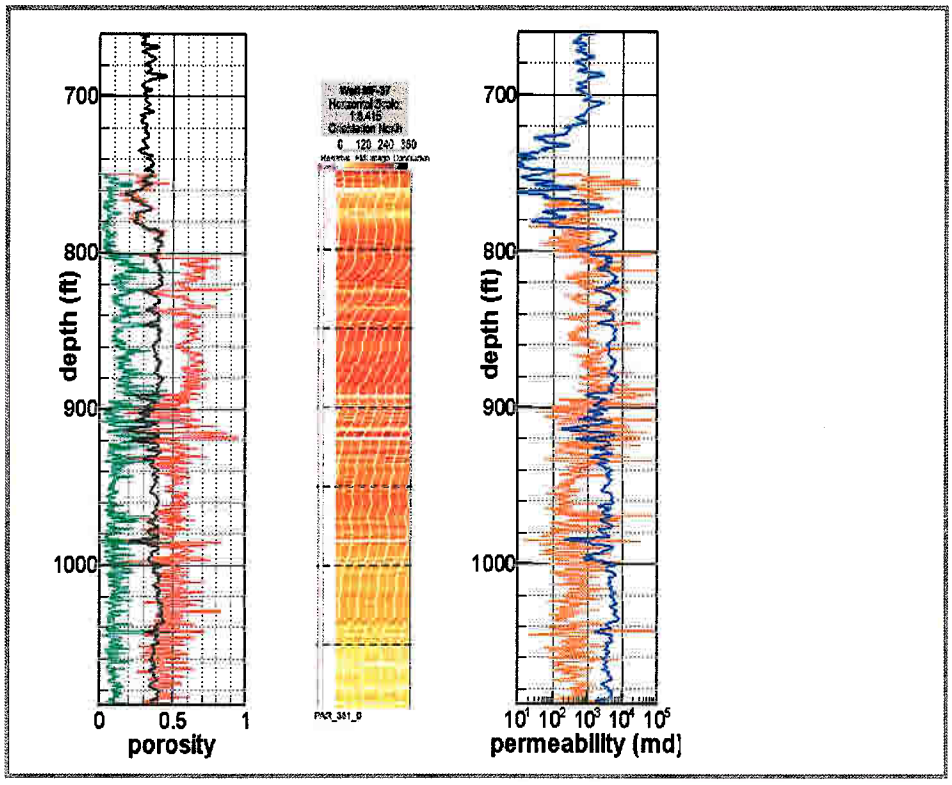

FIGURE 4. Comparison between the FMI image log and the porosity and permeability well logs of well MF-37. The porosity logs illustrate the effects of secondary porosity on matrix and total porosity. The dark log is the ELAN porosity. The last track shows the intrinsic permeability (blue) and KTIM permeability logs.

III. INTERPRETATION OF INTERWELL IMAGES

A. Spectral Analysis

The zero-vertical offset waveforms were extracted from the crosswell seismic data set to identify zones of high attenuation. Figure 5 shows a comparison of these waveforms with well logs from well EXPM-1. In the zone from 900 to 950 ft., the waveforms are practically absent (strongly attenuated), and the corresponding spectral plot shows energy losses (see Figure 6). A comparison of the waveforms and the logs illustrates that the high attenuation corresponds to strong variability of the porosity log at 900 to 950 ft. In this interval, the FMI image data shows a horizontal sequence of dark and white streaks. The white streaks are thin resistive units, and the dark streaks are high conductivity features. The resistive units are tight limestone or dolomite, and the high conductive features are porous and saturated with brackish water. The high attenuated zone affected processing of the Stoneley wave signal and prevented the use of permeability logs for generating the permeability image of the interwell region between wells EXPM-1 and MF-37 (i.e., the formation's heterogeneous conditions were not suitable for extracting a reliable permeability log from the sonic data).

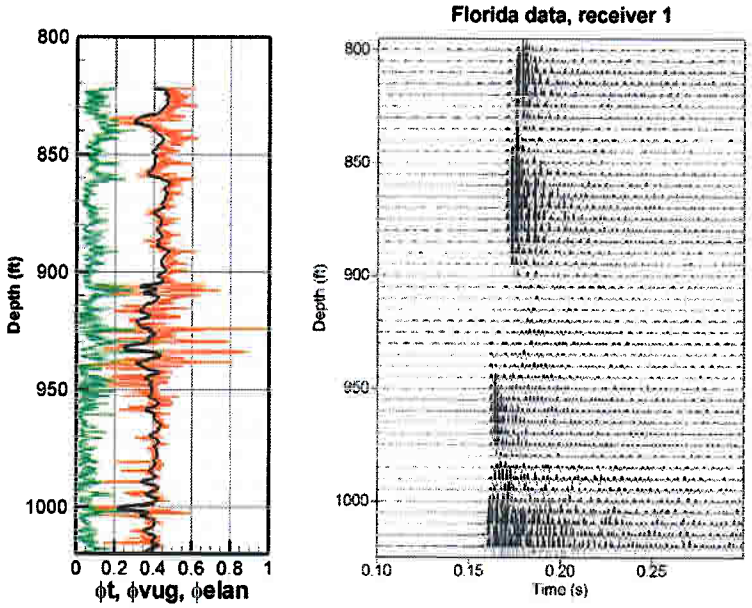

FIGURE 5. Comparison of zero vertical offset waveforms with secondary porosity, total porosity, and average matrix porosity.

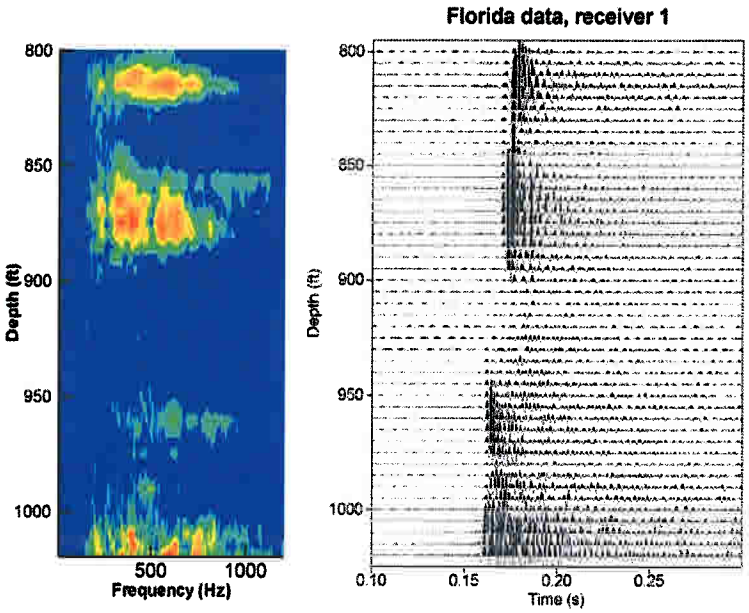

FIGURE 6. Comparison of zero vertical offset waveforms with their spectra.

B. Impedance Image

We inverted the incident reflection seismogram in Figure 2 for impedance using the Vp and density logs and the band-limited method (Olderburg et al., 1983). We constrained the impedance using the velocity and density logs of wells EXPM-1 and MF-37, and we performed the control inversion using linear programming. The inversion was done trace by trace, and its required reprocessing included data checks and possible corrections. The resulting impedance image in Figure 7 shows the variation of the pore structure and other features more clearly than the reflection or tomography data alone. The derived impedance from sonic and density logs of the wells was superimposed in the impedance image to illustrate the crosswell seismic resolution versus the well log resolution.

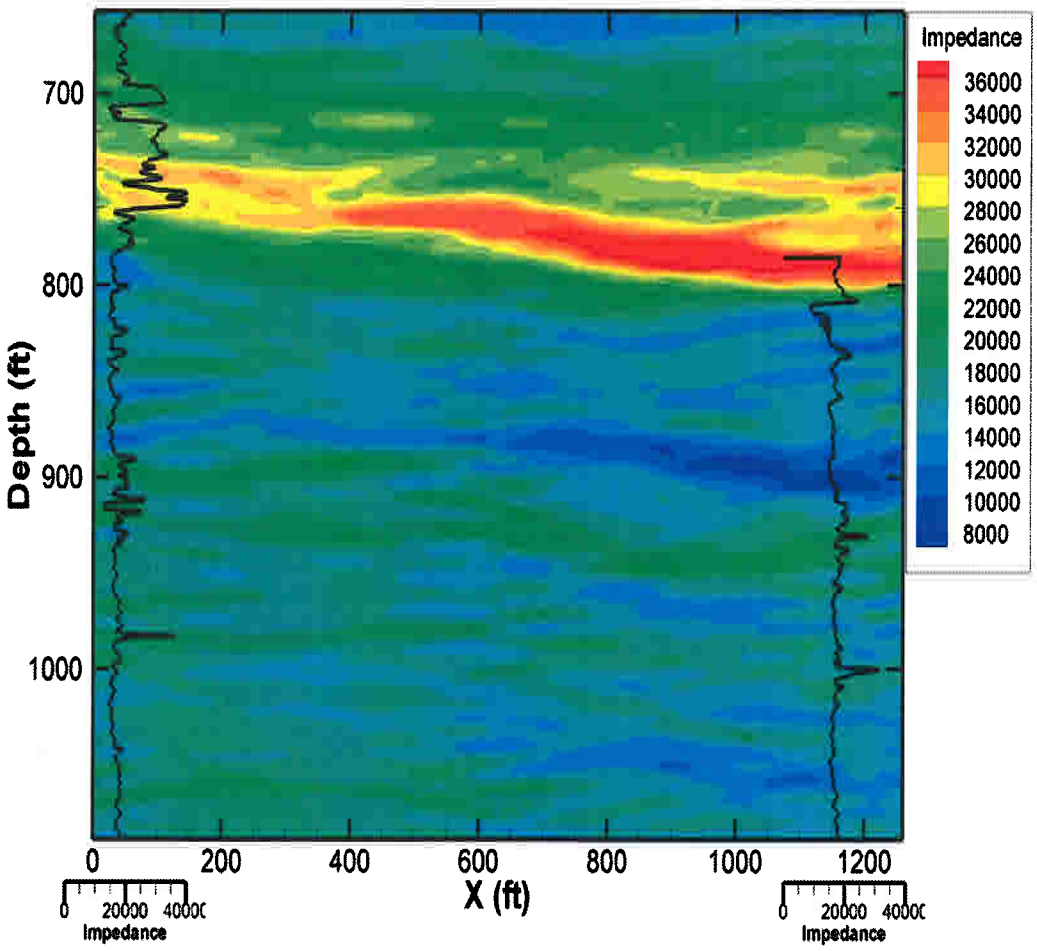

FIGURE 7. P-wave impedance computed from crosswell reflection data. The well log impedance from wells MF-37 and EXPM-1 are superimposed at the well locations to provide better visual comparison to the surface seismic impedance.

In the regions slightly above 800 ft. and 1090 ft. (see Figure 7), we observed a light blue continuous background that corresponded to a low impedance formation; superimposed on this background are more rigid heterogeneities represented by dark green features. Slightly above 900 ft., we observed a low impedance zone (low velocity and density) that is continuous between both wells and softer in the region near well EXPM -1. Below this zone there is an increase of impedance that can be observed in both well logs. This 25-ft. zone is formed by two separate structures (green) that converge into one unit 800 ft. from well MF-37. At this point, there are still discontinuities that slightly separate the two structures. The presence of this single unit can be observed in the impedance well log signature in well EXPM-1, which is represented by a single maximum impedance. The third important feature observed in the impedance image is the high impedance unit above 800 ft. This is a continuous zone that can be considered a low permeability confining unit or permeability barrier.

C. Cross Plots, Porosity and Permeability Images

We created cross plots between impedance and permeability and porosity logs to derive regression equations at the borehole location. We used the resulting relationships to generate permeability and porosity images at the crosswell seismic scale. Based on the permeability well log evaluation, we selected the permeability logs: the FMI-derived permeability (KTIM) and the intrinsic ELAN intrinsic permeability (KINT). The cross plot between the KTIM and the impedance is given in Figure 8(a), and the cross plot between the KINT and the impedance is given in Figure 8(b). Since the KTIM permeability is uncorrelated with impedance, and the KINT perfectly correlates with impedance, we picked the ELAN regression equation given by

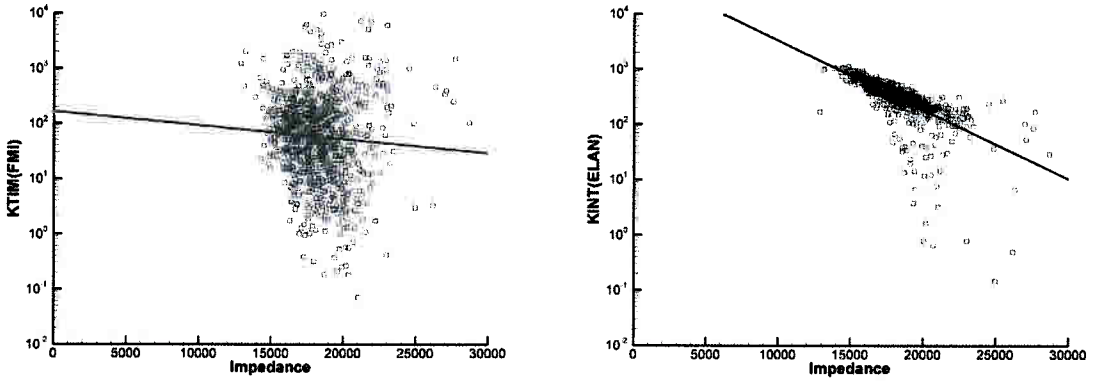

FIGURE 8. (a) Cross plot of well log impedance with FMI permeability. (b) Cross plot of well log impedance with intrinsic permeability.

$$\text{KINT} = \exp(-2.88\text{e-}4\ Z + 11.0) \tag{1}$$

Where KINT is in millidarcies and Z is the impedance in $(g/cm^3)(feet/s)$. In similar form, we cross plotted the porosity with the impedance log. The resulting equation is given by

$$\text{PHIT} = 0.754 - 2.01\text{e-}5\ Z \qquad \textit{volume of fraction} \tag{2}$$

The two cross plots are given in Figures 8(b) and 9. As expected, porosity increases as impendence decreases. Matrix permeability also decreases inversely with impedance. In fact, the permeability correlates directly with the porosity.

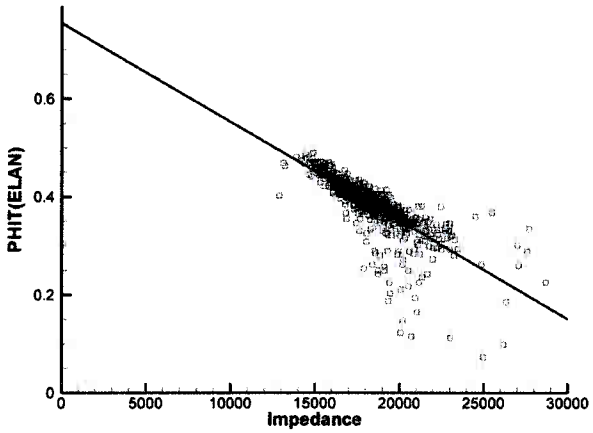

FIGURE 9. Cross plot of well log impedance with total porosity log.

To convert the impedance section to porosity and permeability images, we used the regression equations for porosity versus impedance and permeability versus impedance given by Equations 1 and 2, respectively. Each pixel of the impedance images is converted to porosity and permeability by replacing its value in the proper relationship given either by Equation 1 or 2. The porosity image in Figure 10 is obtained by placing the porosity values given in Figure 7 into the regression Equation 2. In a similar way, the permeability image is determined by inserting the impedance values given in Figure 7 into regression Equation 1. Thus, the correlation equations used to map the impedance images into porosity and permeability reflect structural changes within the limestone formation at depth. The images (see Figure 10 and 11) contain the corresponding well logs, and their resolution can be compared with the well logs that overlay them.

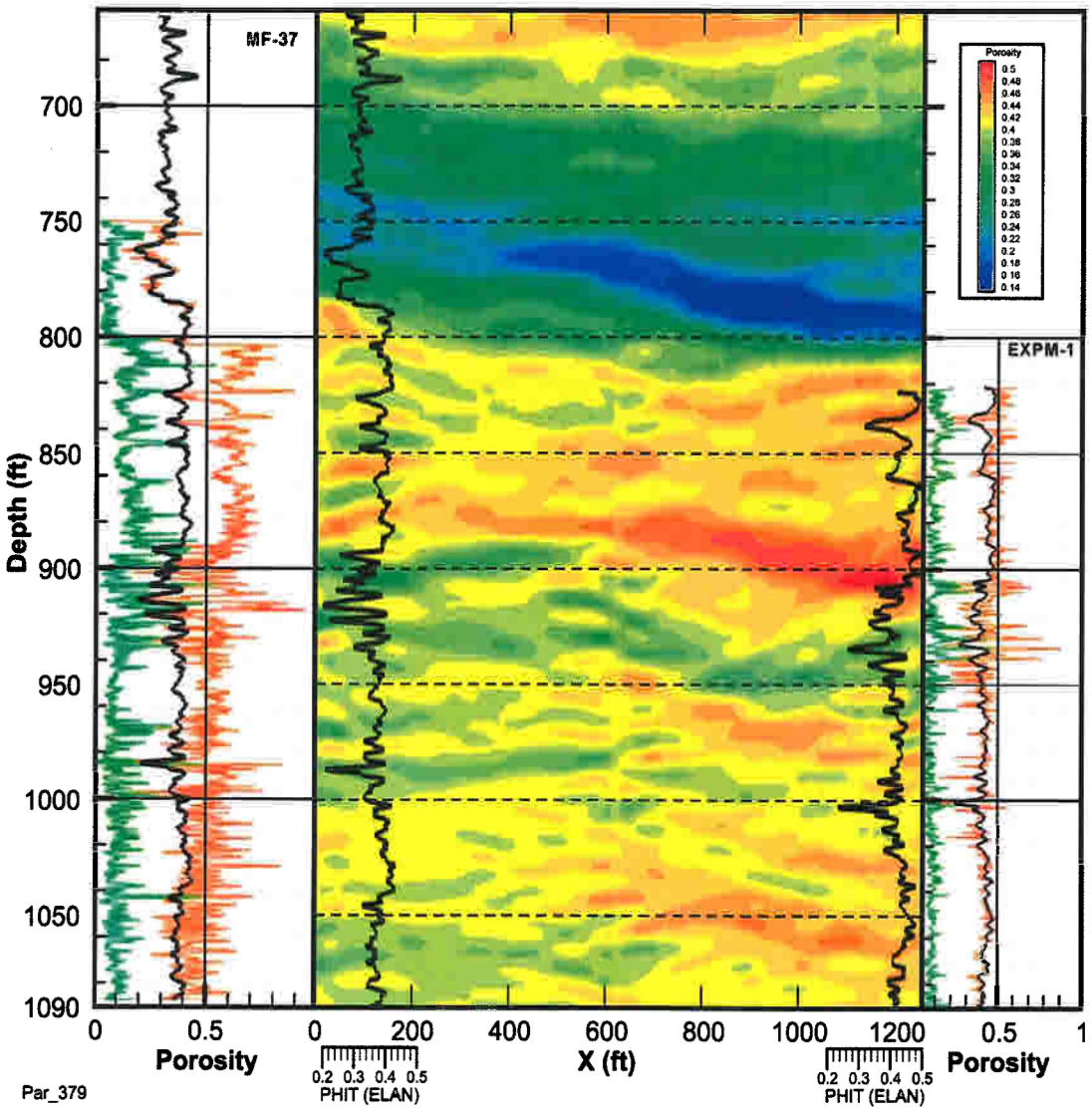

FIGURE 10. Comparison of the porosity image and porosity logs of wells MF-37 and EXPM-1.

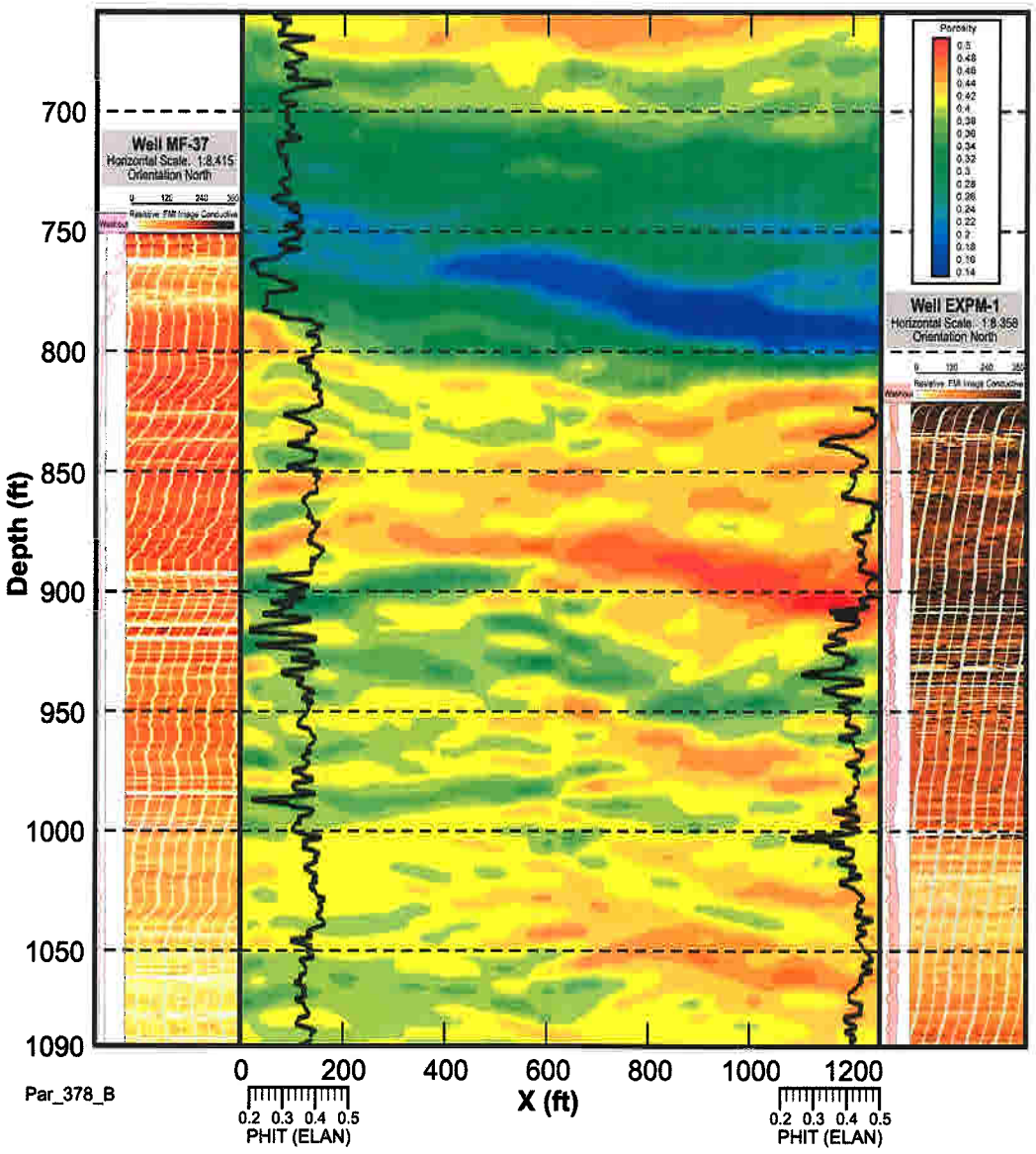

FIGURE 11. Comparison of the porosity image and FMI images of wells MF-37 and EXPM-1.

D. Porosity Image

The porosity image was integrated with FMI image logs and also with porosity well logs from both wells. Figure 10 illustrates the comparison of the total porosity image and the FMI image logs from both wells. The ELAN porosity logs correlate well with several horizontal streaks (resistive units) in both wells. This comparison shows that the resistive units are connected between the wells. The FMI image logs are capable of capturing these features by themselves. The porosity image does not distinguish these features, but does reveal lateral variations of the matrix porosity. In particular, a highly porous interval at 800 to 900 ft. is continuous, with porosities ranging from 0.38 to 0.5 volume fraction. Near well EXPM-1, a high porosity anomaly (red) correlates with a high conductivity FMI interval at 890 to 910 ft. The high FMI conductivity intervals are controlled by the saturated porous zones with brackish water. Such conditions were observed in water samples from the wells, and are more pronounced in well EXPM-1 than well MF-37.

Figure 11 illustrates the different porosities and the interwell porosity image. The well logs show that the region of well MF-37 contains more secondary porosity than the region of well EXPM-1, and that the matrix porosity is relatively constant. In spite of this, the secondary porosity is greater in the interval from about 900 to 950 ft. Based on the porosity well logs, the secondary porosity makes a strong contribution to the FMI porosity, or total porosity in the interval of 800 to 900 ft. This is the zone with the most water production, according to fluid-type logs (Bennett and Recrewald, 2002). The porosity image shows the lateral variability of the matrix and the major boundaries of this interval. It is possible that the secondary porosity interconnects with the matrix porosity to yield good water production in the interval from 800 to 900 ft. between both wells.

In the above interval, the matrix porosity decreases (shown in green in Figure 11), which corresponds to a stiffer zone than the upper and lower adjoining areas. In this stiff carbonate, the secondary porosity is much higher than in the rest of the formation; this may be due to the brittle limestone conditions. However, this zone was not addressed by Bennett and Recrewald (2002) to be a higher water production flow unit. This suggests that the secondary porosity peaks in this 25-foot interval are located near the region surrounding the borehole only, and not interconnected with the matrix in the interwell region. The same characteristics are observed in well EXMP-1. However, in the region below 930 ft., we observe a more uniform FMI total porosity log that extends all the way to 1090 ft. In this interval, the porosity has a similar signature as in the 800 to 900 ft. interval, and the secondary porosity makes a strong contribution to water production, particularly in well MF-37.

E. Permeability Image

To further investigate the matrix interconnectivity, we analyzed the permeability based on the FMI data. The permeability was estimated using the Timur-Coates equation and data sets from both wells. The Timur-Coates equation estimates secondary porosity by considering free water and matrix porosity from the FMI data. The plots of Figures 3 and 4 capture the fluid-flow conduits that cannot be resolved with the sonic data. We attempted to correlate the resulting

permeability log with the impedance, but we found that the two logs do not correlate. This was expected, because P-wave velocity data has much lower resolution than the permeability data based on the FMI data. The permeability image in Figure 12 was integrated with the permeability logs from both wells, which are superimposed on the image.

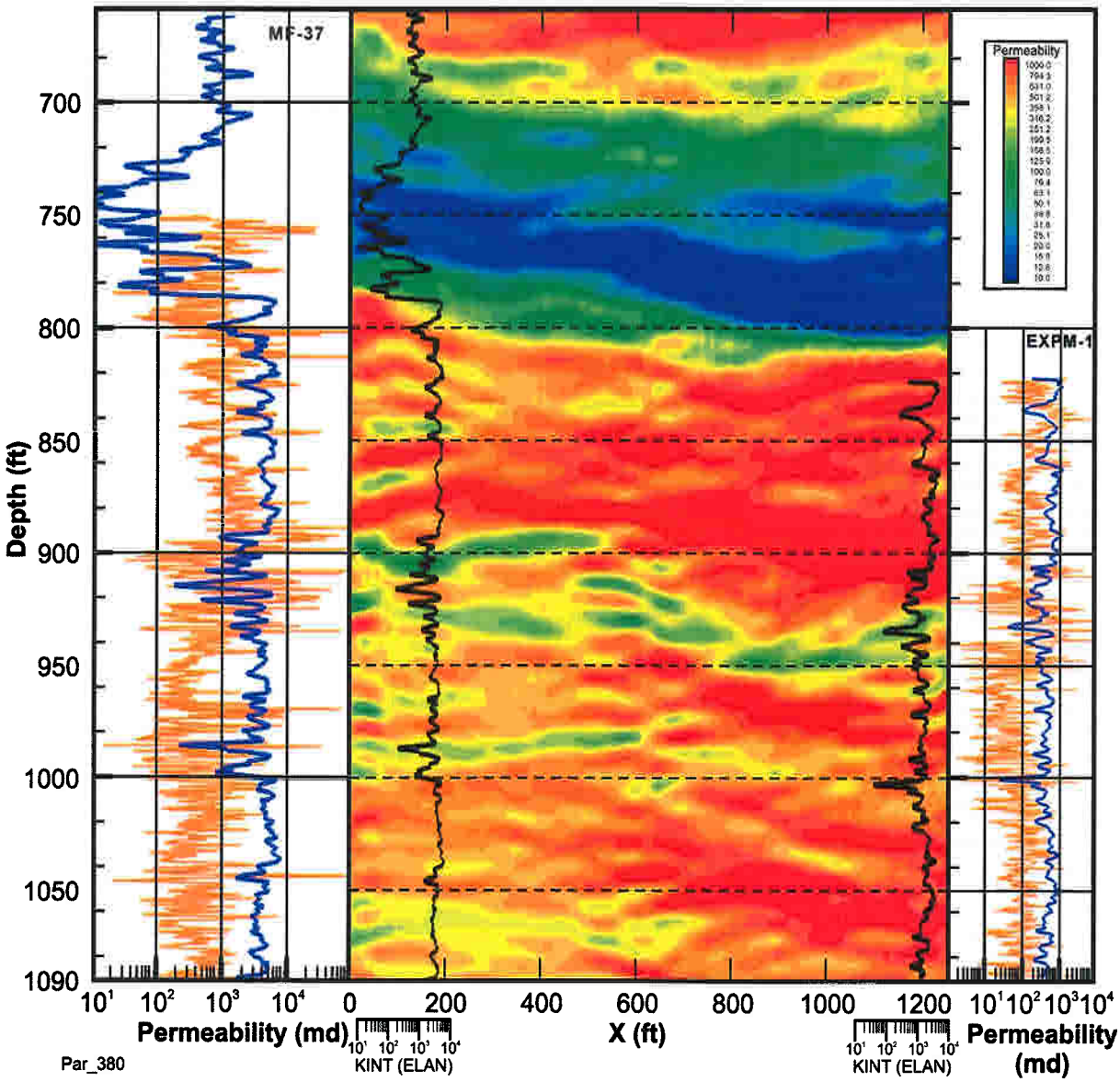

FIGURE 12. Comparison of the permeability image and FMI images of wells MF-37 and EXPM-1.

Both logs show a similar signature in the zone from 900 to 950 ft. This is the zone of higher impedance that is shown in green in Figure 7. This zone has an average permeability of 230 millidarcies (md) that is surrounded by a matrix permeability of about 1000 md. The zone of 230 md is associated with an impedance of 27000, and the red zone corresponds to about 13000. The zone with lower permeability is twice as stiff as the region with higher permeability. This stiffer limestone might be more brittle than the region of high matrix permeability, and could easily be broken or fractured, meaning that conduits could easily be formed. This may be why high permeability features were captured by the FMI-based logs for both wells in the same zone – permeability reaching values up to 100,000 md in well MF-37 and 10,000 md in well EXPM-1. Since water production appears to be low in the 900 to 930 ft. interval, it is possible that higher permeability values captured by the FMI permeability logs are localized in the region near the borehole and do not extended to well EXPM-1. The two zones of high water production are better visualized by the red color in the permeability image than any other image. Although this image in Figure 12 illustrates only the variability of matrix permeability, it allow us to integrate the high resolution well log information by evaluating how secondary porosity can contribute to high water production in the interwell region intervals from 800 to 900 ft. and 930 to1050 ft.

IV. DISCUSSION AND CONCLUSIONS

To make use of the high resolution permeability logs, we compared the porosity/permeability images in Figures 11 and 12 with the permeability logs based on FMI at a 3-inch resolution. These plots show the zones not captured by the crosswell data as well as those that were captured. The correlation of logs from both the wells shows a degree of continuity in the small features. The plots help us identify zones that are connected between the wells, and how the high permeability conduits are embedded in the formation matrix. Our interpretation allows us to estimate matrix permeability and porosity variations at the interwell scale. Indirectly, we are also able to assess whether the conduits are connected. The results can be useful when characterizing formations that contain conduits by using well log information and crosswell data.

The high resolution FMI logs reveal secondary porosity features that are associated with high permeability zones and high water production in the FAS at intervals from 800 to 900 and 930 to 1090 ft. The crosswell images reveal variability in matrix porosity and permeability, which leads us to conclude that interconnectivity exists between the secondary and primary porosities in the interwell region. However, in the interval from 900 to 930 ft., the FMI images indicate that the secondary porosity does not have good interconnectivity with the matrix porosity. Additional indicators of this are that water production is lower in this interval, and the interwell image is heterogeneous and discontinuous.

Crosswell seismic reflection data gives information on the intrinsic properties of the formation, but it cannot resolve small features such as the conduits and fractures seen in the FMI data. The FMI data can capture such features at a resolution of 1 to 3 inches, which cannot even be accomplished by sonic log data. For example, in the FMI of Figure 11, the dark features observed in well EXPM-1 correspond to lower electrical resistivity and to fluid-filled pores/vugs/fractures or clay-reach zones. The permeability estimated on the basis of the FMI data represents fluid flow through the conduits, which also correlates with the zones of greater water production.

The zero vertical offset data exhibits zones of high attenuation that correlate with the FMI data. In particular, the variability of the formation at the borehole wall is reflected in the high attenuation. This suggests that the wave attenuation is sensitive to the presence of conduits. In fact, the macro-porosity, which is a combination of fractures, vugs, collapse features, conduits and other large pore structures, is visible with the FMI. In the interval from 900 to 950 ft., these features contribute to scattering attenuation that may be observed in the zero vertical offset waveforms and the spectra. This heterogeneous low velocity zone is delineated by as a green feature in the crosswell permeability and impedance images. In the zone of high permeability or high water production, the zero vertical offset waves are not strongly attenuated, and any contribution to the waveform characteristics is due to the intrinsic permeability or fluid flow effects. These scattering and intrinsic effects can be explained by modeling the wave phenomena in the interwell region.

V. SUMMARY

- The crosswell seismic image shows zones of high water production and high matrix porosity and permeability.

- The top of the FAS and the lower boundary of the intermediate confining unit (the basal Hawthorn) are delineated with the impedance image.

- The spectral waveform analysis identifies the heterogeneous zone at the interval from 900 to 950 ft. This is one of the main zones that prevented the use of Stoneley wave permeability. The relationship between well logs and the zero vertical offset waveforms suggests that the wave attenuation in this interval is due to scattering associated with the vertical variability of the secondary and primary porosity sequence in the 900 to 950 ft. interval.

- The impedance, porosity and permeability images clearly show the variation of the aquifer matrix in the interwell region.

- The impedance image identifies stiff and soft zones. The stiff zones contain conduits that may not be connected, which are associated with secondary porosity features such as pore/vugs/fractures near the wells. The soft zones of low impedance are associated with high water production.

- The impedance and porosity images, combined with the FMI image logs, can provide information of the development of conduits in the stiff intervals.

- The permeability image provides a good visualization of low and high matrix permeability distribution intervals.

- The FMI image data provides information on the secondary porosity distribution at the borehole scale that cannot be detected with any other log. In particular, the FMI shows a sequence of dark (conductive) and white (resistive) bands. The conductive bands are porous and saturated with salt water (high permeability spikes). Some of the resistive bands may be connected between wells, but the dark zones embedded in the white bands are not. Zones characterized by these sequences are intervals with low water production.

VI. REFERENCES

Bennett, M.W., and Recrenwald, E.E., 2002, Hydrogeologic investigation of the Floridan Aquifer System, Port Mayaca Site, Martin County, Florida: Preliminary Report, SFWMD, West Palm Beach.

Olderburg, D.W, Scheuer, T., and Levy, S., 1983, Recovery of the acoustic impedance from reflection seismograms, *Geophysics*, **48**, 1318-1337.

Parra, J.O., Hackert, C.L., and Bennett, M.W., 2003, Permeability and porosity images based on NMR, sonic, and seismic reflectivity: Application to a carbonate aquifer, *The Leading Edge*, **22**(11), 1102-1108.